

Analytical Techniques for the Doppler Signature of Sea Surfaces in the Microwave Regime—I: Linear Surfaces

Frédéric Nouguier, Charles-Antoine Guérin, and Gabriel Soriano

Abstract—This paper is the first in a series of two papers on the use of combined improved hydrodynamic and electromagnetic analytical models for the simulation of the ocean Doppler spectrum at microwave frequencies. Under a linear assumption for the sea surface, we derive statistical expression for the main Doppler characteristics according to asymptotic scattering models. We consider classical models such as the Kirchhoff approximation and the two-scale model, as well as the more recent weighted curvature approximation (WCA). We recover two salient features of Doppler signature in the microwave regime. First, the Doppler characteristics are very sensitive to polarization, with higher mean Doppler shift in horizontal polarization. This is correctly rendered by the WCA but not the classical models. Second, the first two moments of the Doppler spectrum exhibit a nontrivial dependence on incidence angle. Results compare favorably with rigorous numerical computations for 1-D surfaces published in the literature. The simplicity and accuracy of the analytical models provide a valuable tool for the Doppler analysis of 2-D sea surfaces.

Index Terms—Doppler spectrum, gravity waves, microwave, remote sensing, rough surfaces, scattering, sea surface.

I. INTRODUCTION

THE DOPPLER analysis associated to the backscattered radar return from the sea surface is a very valuable tool in ocean remote sensing. The Doppler spectrum indeed carries much more information than a mere radar backscattering cross section under a given incidence and is easily interpretable in terms of wind and current conditions for HF radio waves (e.g., [1] and the references therein). In that case, the dominant mechanism is resonant Bragg scattering, and the mean Doppler shift is imposed by the so-called free Bragg frequency, i.e., the frequency associated to the wave with half the electromagnetic wavelength at grazing incidence. The experimental Doppler spectra are accurately modeled by the perturbative theory of

Barrick and Weber [2], [3], which describes second-order interactions of both the electromagnetic and hydrodynamic processes.

In the microwave regime, Doppler characteristics turn out to be more complex. A large number of field experiments have been conducted in the last 30 years, most of them at grazing incidence because of practical constraints (e.g., [4] for the Ku-band, [5] and [6] for the X-band, and [7] for the L-band). The observed Doppler spectra are usually broader than in the HF regime, with a mean frequency that is sometimes much higher than the free Bragg frequency, depending on wind speed and radar incidence. This effect is more pronounced in horizontal polarization and at large incidences. Today, however, no asymptotic theory is capable of fully explaining and reproducing these experimental observations. The reason is twofold. First, the analytical scattering models [8] have limited range of validity, particularly at larger incidences, and second, the hydrodynamic description of nonlinear short gravity waves is still an open issue. The aim of this paper is to go further in this direction by combining recent and efficient scattering and hydrodynamic analytical models. This task will be decomposed in a set of two companion papers. This first paper will put the emphasis on analytical scattering models, whose potential for the Doppler analysis has, in our opinion, not been fully exploited. To separate electromagnetic and hydrodynamic issues, the sea surface will be assumed linear in this first stage. In a second companion paper, weakly nonlinear analytical models will be combined with the scattering models to reach a complete realistic description of the Doppler spectrum.

The classical approach to tackle the problem relies on the two-scale model (TSM) [9]. More recent results [10]–[13] have shown that modern analytical scattering models can account for some characteristic features of microwave Doppler spectra such as the nontrivial dependence of the central frequency upon the incidence angle and its sensitivity to polarization. However, in using such asymptotic techniques, a tradeoff must be found between the accuracy and robustness of the model and its numerical efficiency. The latter is intimately related to the existence of a statistical formulation for the main Doppler characteristics (central frequency and width), which prevents from time-consuming Monte Carlo simulations. With this idea in mind, we will revisit the classical models, starting with the Kirchhoff approximation (KA) and its two-scale formulation. We will show that extremely simple yet nontrivial formula can be obtained for the central frequency and width of the

Manuscript received November 16, 2010; revised February 24, 2011; accepted March 30, 2011. Date of publication June 22, 2011; date of current version November 23, 2011. This work was supported by ANR Project ANR-09-BLAN-0232-01 SIMODE.

F. Nouguier is with the Laboratoire d'Océanographie Spatiale, Institut Français de Recherche pour l'Exploitation de la Mer, 29280 Plouzané, France.

C.-A. Guérin is with the Laboratoire de Sondages Electromagnétiques de l'Environnement Terrestre (Unité Mixte de Recherche 6017), Geosciences and Remote Sensing Department, Centre National de la Recherche Scientifique/Université du Sud-Toulon-Var, 83957 La Garde, France.

G. Soriano is with the Institut Fresnel (Unité Mixte de Recherche 6133), Centre National de la Recherche Scientifique/Paul Cézanne University Aix-Marseille III, 13397 Marseille, France.

Color versions of one or more of the figures in this paper are available online at <http://ieeexplore.ieee.org>.

Digital Object Identifier 10.1109/TGRS.2011.2152848

Doppler spectrum. These models, however, apply to a limited incidence range and are polarization insensitive. We will show that a more accurate electromagnetic description can be reached with the weighted curvature approximation (WCA) [14], [15], whose recently improved formulation [16] is adapted to a fully analytical derivations of the Doppler spectrum.

The theory will be developed for fully 2-D surfaces, and in most cases, analytical formulas will be given for the central frequency and width of the Doppler spectrum, which can be easily implemented. At this stage, however, our goal is not to produce realistic simulations to be compared with experiments but rather to validate the technique. The numerical validation of this and the subsequent studies will therefore be performed for 1-D surfaces. This makes the illustration easier and renders a comparison possible with the reference work by Toporkov and Brown [17], who realized a set of extensive simulations according to a rigorous electromagnetic model for 1-D surfaces. Therefore, our numerical tests have been designed identical to those presented in [17] and [18], namely, 1-D surfaces with Pierson–Moskowitz (PM) spectrum at L- and X-bands for 5- and 7-m · s⁻¹ wind speeds (at 19.5 m above the sea level). We are aware that more realistic spectra as PM could have been chosen and certainly will be implemented in future steps. However, this choice is imposed for the moment by the necessity of a fair comparison with the previously cited works.

II. OCEAN DOPPLER SPECTRUM

As usual, the sea surface is described by its Cartesian coordinates $z = \eta(\mathbf{r}, t)$, with mean horizontal plane $\mathbf{r} = (x, y)$ and upward-directed vertical axis. From an electromagnetic point of view, the interface separates the upper medium (air), assimilated to vacuum, from the lower medium (water), assumed to be homogeneous and described by its complex permittivity. A fixed coherent radar illuminates the surface at some given frequency and incidence. We assimilate the radar beam to a monochromatic plane wave with wave vector \mathbf{K}_0 , so that $\hat{\mathbf{K}}_0$ will also denote the radar look direction (here and everywhere, we use the notation $\hat{\mathbf{u}} = \mathbf{u}/\|\mathbf{u}\|$ for the direction of a vector). Denoting $\mathbb{S}(t)$ as the backscattered amplitude from the frozen surface at time t (we refer to [8] for the exact definition), the time covariance function of the backscattered field is the limit of the statistical average

$$\mathcal{C}(t) = \frac{4\pi}{|A|} \left(\langle \mathbb{S}(t)\mathbb{S}^*(0) \rangle - |\langle \mathbb{S}(0) \rangle|^2 \right) \quad (\text{II.1})$$

for an infinite illumination area $|A|$. Note that $\mathcal{C}(0)$ is the classical definition of the normalized radar cross section (NRCS). The Doppler spectrum is the corresponding Fourier transform

$$D(\omega) = \int_{\mathbb{R}} e^{-i\omega t} \mathcal{C}(t) dt \quad (\text{II.2})$$

and $f = \omega/(2\pi)$ is the Doppler frequency shift. Waves traveling away from the radar mainly contribute to negative Doppler shifts, while waves traveling toward the radar mainly create positive shifts. Thus, Doppler spectra usually contain two peaks with different amplitudes, depending on the radar look

direction. This is shown in Fig. 1(a). For 1-D surfaces, it is customary to consider one-sided sea spectra corresponding to waves traveling to the left (or right) direction. In that case, the Doppler spectrum is centered around some positive (or negative) peak frequency, and the Doppler centroid f_c and width γ can be defined through the first two moments of the spectrum

$$\begin{aligned} f_c &= \frac{\omega_c}{2\pi} = \frac{1}{2\pi} \frac{\int_{\mathbb{R}} \omega D(\omega) d\omega}{\int_{\mathbb{R}} D(\omega) d\omega} \\ \gamma^2 &= \frac{1}{(2\pi)^2} \frac{\int_{\mathbb{R}} \omega^2 D(\omega) d\omega}{\int_{\mathbb{R}} D(\omega) d\omega} - f_c^2. \end{aligned} \quad (\text{II.3})$$

The notion of one-sided spectrum can be extended to the case of 2-D surfaces by artificially restricting the sea spectrum to waves traveling toward (or away from) the radar. This amounts to keeping wave directions in the same (or opposite) half-plane as the radar look direction $\hat{\mathbf{K}}_0$, as shown in Fig. 1(b). Positive shift is arbitrarily chosen and implies that the propagation half-plane is defined by $\text{sgn}(\hat{\mathbf{K}}_0 \cdot \hat{\mathbf{k}}) < 0$, where $\hat{\mathbf{k}}$ is the considered wave direction and sgn is the sign function ($\text{sgn}(x) = \pm 1$ if $x \gtrless 0$). Note that we thereby ignore the contribution of waves traveling away from the radar to positive frequencies and *vice versa*. In reality, the spectral density varies continuously as a function of the azimuth angle with respect to the wind direction, and the notion of half-sided spectrum is purely artificial. In the practical case of a two-sided spectrum, there are two Doppler centroids along and against the wind direction. Under these circumstances, the definition of a central peak through the first moment is irrelevant as sign cancellations in the integral will produce some meaningless intermediate value. The solution is to calculate the center of each peak for the two half spectra separately. One should keep this in mind when using the main results of this paper.

III. TIME-EVOLVING LINEAR SEA SURFACE

Without loss of generality (waves propagate in all directions), we can represent a linear time-dependent surfaces in the following form:

$$\eta(\mathbf{r}, t) = \int_{\mathbb{R}^2} d\mathbf{k} [a(\mathbf{k})e^{-i\omega_{\mathbf{k}}t} + a^*(-\mathbf{k})e^{i\omega_{\mathbf{k}}t}] e^{i\mathbf{k}\cdot\mathbf{r}} \quad (\text{III.4})$$

where $a(\mathbf{k})$ is the complex amplitude of the wave, \mathbf{k} is the associated wavenumber, and $\omega_{\mathbf{k}} = \sqrt{g|\mathbf{k}|(1 + |\mathbf{k}|^2/k_M^2)}$ is the gravity–capillarity dispersion relationship ($k_M = 363.2 \text{ rad} \cdot \text{m}^{-1}$ is the wavenumber with minimum phase speed). In the linear assumption, the phases of the different complex amplitudes are supposed to be uncorrelated. Denoting $\rho(\mathbf{r}, t) = \langle \eta(\mathbf{r}, t)\eta(\mathbf{0}, 0) \rangle$ as the spatiotemporal covariance function of the surface, it follows that

$$\rho(\mathbf{r}, t) = \int_{\mathbb{R}^2} d\mathbf{k} [\Gamma_a(\mathbf{k})e^{-i\omega_{\mathbf{k}}t} + \Gamma_a(-\mathbf{k})e^{i\omega_{\mathbf{k}}t}] e^{i\mathbf{k}\cdot\mathbf{r}} \quad (\text{III.5})$$

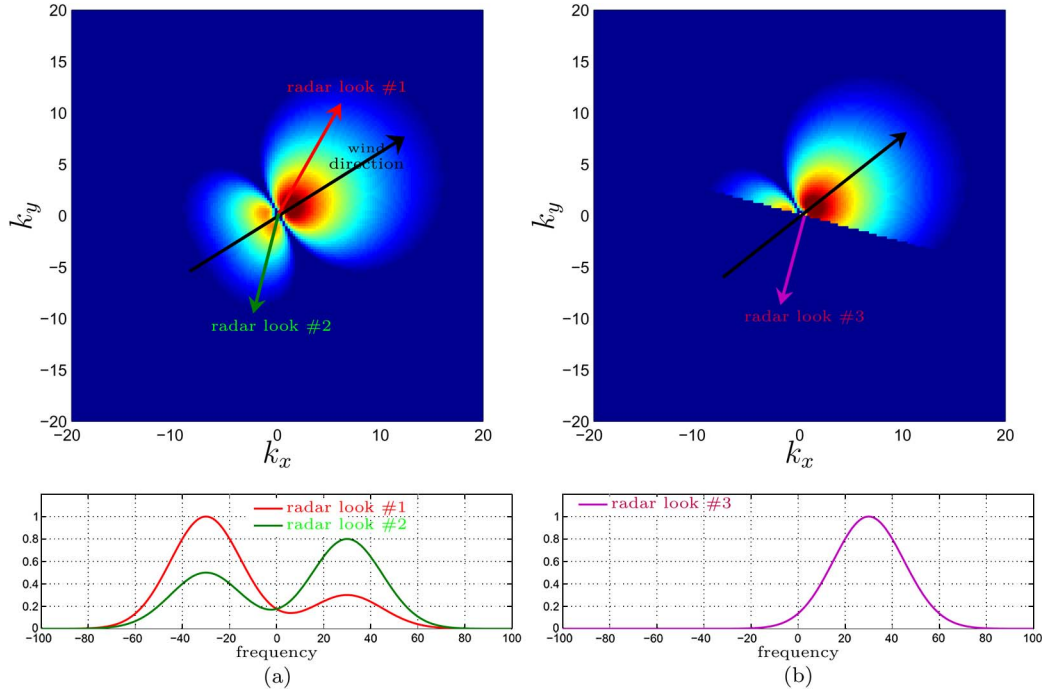


Fig. 1. Norm of the wave complex amplitude: Γ_a in wavenumber space (k_x, k_y) . Three radar looking directions and their corresponding Doppler spectra are shown. (a) Full spectrum. (b) Half-sided spectrum.

where $\Gamma_a(\mathbf{k})$ defined by $\langle a(\mathbf{k})a^*(\mathbf{k}') \rangle = \Gamma_a(\mathbf{k})\delta(\mathbf{k} - \mathbf{k}')$ is the square amplitude of waves traveling in different azimuthal directions. Assuming the waves to travel only toward (or away from) the radar is equivalent to supposing that $\Gamma_a(\mathbf{k})$ vanishes in the half-space of wavenumber pointing to the radar look direction ($\hat{\mathbf{k}} \cdot \hat{\mathbf{K}}_0 > 0$), i.e., Γ_a is half sided. Using this assumption, (III.5) can be rewritten as

$$\rho(\mathbf{r}, t) = \int_{\mathbb{R}^2} d\mathbf{k} \Gamma(\mathbf{k}) e^{i(\mathbf{k} \cdot \mathbf{r} + \text{sgn}(\hat{\mathbf{k}} \cdot \hat{\mathbf{K}}_0) \omega_{\mathbf{k}} t)} \quad (III.6)$$

where $\Gamma(\mathbf{k}) = \Gamma_a(\mathbf{k}) + \Gamma_a(-\mathbf{k})$ is the usual centrosymmetric wave vector spectrum.

Fig. 2 shows an example of the spatiotemporal covariance function $\rho(x, t)$ for 1-D surfaces with wind speed $U_{19.5} = 7 \text{ m} \cdot \text{s}^{-1}$. Along this paper, we use the omnidirectional PM spectrum $\Gamma(k) = (1/2)\Gamma_{\text{PM}}(|k|)$, where

$$\Gamma_{\text{PM}}(k) = \frac{\alpha}{2|k|^3} \exp\left\{-\frac{\beta g^2}{k^2 U_{19.5}^4}\right\} \quad (III.7)$$

with $\alpha = 8.1 \cdot 10^{-3}$ and $\beta = 0.74$. The extra factor 1/2 accounts for the fact that energy is equally spread over both positive and negative axes. Note that this is different from [17], which chose the half-sided PM spectrum (i.e., (III.7) for positive k only; zero if otherwise). However, in our basic assumption that the negative wavenumbers do not contribute to positive Doppler shifts, this amounts to the same. Again, we insist on the fact that the choice of the PM spectrum along this work is imposed

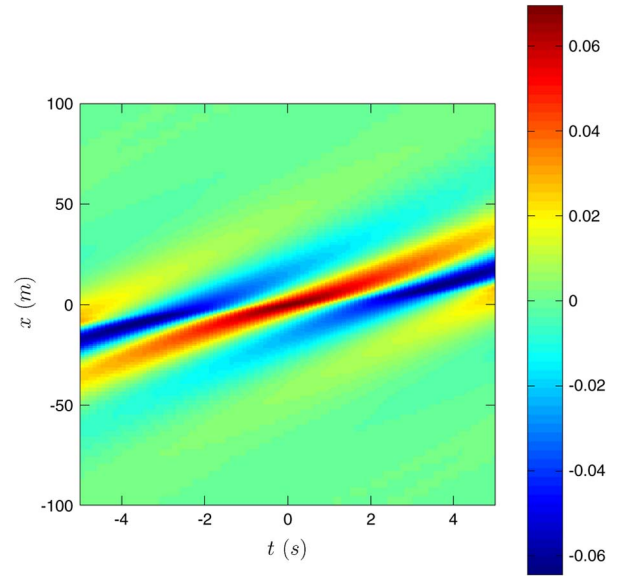


Fig. 2. One-dimensional spatiotemporal covariance function of elevation: $\rho(x, t)$ at $U_{19.5} = 7 \text{ m} \cdot \text{s}^{-1}$ wind speed.

by the first stage of validation after the results in [17], even if it is less realistic than some more recent spectra.

In both cases, waves are traveling in the positive x -direction only ($K_0 < 0$). We note in passing that the covariance function oscillates both in time and space and is localized around the diagonal $k_p x - \omega_{k_p} t = 0$, where k_p is the peak frequency. As a consequence, its spatial range varies with time. This makes the computation of the field covariance function (see (IV.9) further) more difficult than an ordinary NRCS.

IV. KA

The backscattered amplitude in the KA [19] is given by

$$\mathbb{S}_{\text{KA}}(t) = \frac{\mathbb{K}}{Q_z} \int_{\mathbb{R}^2} \frac{d\mathbf{r}}{(2\pi)^2} e^{i\mathbf{Q}_H \cdot \mathbf{r}} e^{iQ_z \eta(\mathbf{r}, t)} \quad (\text{IV.8})$$

where we have introduced the so-called Ewald vector $\mathbf{Q} = -2\mathbf{K}_0$, together with its horizontal and vertical projections \mathbf{Q}_H and Q_z , respectively. Here, \mathbb{K} is the Kirchhoff kernel whose expression can be found in, e.g., [8]. If the surface is assumed to be a Gaussian random process, a classical calculation leads to the following expression for the field time covariance function:

$$\begin{aligned} \mathcal{C}_{\text{KA}}(t) &= \frac{1}{Q_z^2} \frac{|\mathbb{K}|^2}{\pi} \int_{\mathbb{R}^2} d\mathbf{r} e^{i\mathbf{Q}_H \cdot \mathbf{r}} \left[e^{-Q_z^2(\rho(\mathbf{0}, 0) - \rho(\mathbf{r}, t))} - e^{-Q_z^2 \rho(\mathbf{0}, 0)} \right]. \end{aligned} \quad (\text{IV.9})$$

The Doppler spectrum at every incidence angle can be computed in a three-step procedure through successive evaluations of the spatiotemporal covariance function, the field covariance function $\mathcal{C}_{\text{KA}}(t)$, and its Fourier transform. The Doppler central frequency (f_c) and width (γ) can then be obtained through the moments (II.3). Numerical details are given in Appendix B. However, in the KA framework, a more direct derivation of these quantities can be made by noting that

$$\int_{\mathbb{R}} \omega D(\omega) d\omega = -i \left. \frac{\partial \mathcal{C}}{\partial t} \right|_{t=0} \quad (\text{IV.10})$$

$$\int_{\mathbb{R}} \omega^2 D(\omega) d\omega = - \left. \frac{\partial^2 \mathcal{C}}{\partial t^2} \right|_{t=0} \quad (\text{IV.11})$$

which leads to

$$2\pi f_c = -i Q_z^2 N^{-1} \int_{\mathbb{R}^2} d\mathbf{r} e^{i\mathbf{Q}_H \cdot \mathbf{r}} \partial_t \rho(\mathbf{r}, 0) e^{-Q_z^2(\rho(\mathbf{0}, 0) - \rho(\mathbf{r}, 0))} \quad (\text{IV.12})$$

$$\begin{aligned} (2\pi\gamma)^2 + \omega_c^2 &= -Q_z^2 N^{-1} \int_{\mathbb{R}^2} d\mathbf{r} e^{i\mathbf{Q}_H \cdot \mathbf{r}} \left[\partial_{t^2} \rho(\mathbf{r}, 0) + Q_z^2 (\partial_t \rho(\mathbf{r}, 0))^2 \right] \\ &\times e^{-Q_z^2(\rho(\mathbf{0}, 0) - \rho(\mathbf{r}, 0))} \end{aligned} \quad (\text{IV.13})$$

where

$$N = \int_{\mathbb{R}^2} d\mathbf{r} e^{i\mathbf{Q}_H \cdot \mathbf{r}} \left[e^{-Q_z^2(\rho(\mathbf{0}, 0) - \rho(\mathbf{r}, 0))} - e^{-Q_z^2 \rho(\mathbf{0}, 0)} \right] \quad (\text{IV.14})$$

$$\partial_t \rho(\mathbf{r}, 0) = i \int_{\mathbb{R}^2} d\mathbf{k} \operatorname{sgn}(\hat{\mathbf{K}}_0 \cdot \hat{\mathbf{k}}) \omega_{\mathbf{k}} \Gamma(\mathbf{k}) e^{i\mathbf{k} \cdot \mathbf{r}} \quad (\text{IV.15})$$

$$\partial_{t^2} \rho(\mathbf{r}, 0) = - \int_{\mathbb{R}^2} d\mathbf{k} \omega_{\mathbf{k}}^2 \Gamma(\mathbf{k}) e^{i\mathbf{k} \cdot \mathbf{r}}. \quad (\text{IV.16})$$

Equations (IV.15) and (IV.16) are derived from (III.6), but their general forms can be derived from the expression of ρ at (III.5). Hence, under the KA and the linear assumption for the sea surface, the central Doppler frequency and its width can be calculated at the same cost as a classical NRCS.

V. DOPPLER SPECTRUM IN THE TSM APPROXIMATION

In order to derive fully analytical expressions for the Doppler centroid and width in the framework of the KA, we use a two-scale argument in a way very similar to that in [9]. We decompose the spectrum into small- and large-scale components $\Gamma_a = \Gamma_{aL} + \Gamma_{as}$. We call ρ_L and ρ_s , respectively, the corresponding covariance functions

$$\rho_{s/L}(\mathbf{r}, t) = \int_{\mathbb{R}^2} d\mathbf{k} \left[\Gamma_{as/aL}(\mathbf{k}) e^{-i\omega_{\mathbf{k}} t} + \Gamma_{as/aL}(-\mathbf{k}) e^{i\omega_{\mathbf{k}} t} \right] e^{i\mathbf{k} \cdot \mathbf{r}}. \quad (\text{V.17})$$

For sea spectra, a separation frequency around Bragg wavenumber ensures that $Q_z^2 \rho_s(\mathbf{0}, 0) \ll 1$, so we may treat the small scales perturbatively in the exponential

$$\begin{aligned} \mathcal{C}(t) &\simeq \frac{|\mathbb{K}|^2}{\pi Q_z^2} \left(\int_{\mathbb{R}^2} d\mathbf{r} e^{i\mathbf{Q}_H \cdot \mathbf{r}} \left[e^{-Q_z^2(\rho_L(\mathbf{0}, 0) - \rho_L(\mathbf{r}, t))} - e^{-Q_z^2 \rho_L(\mathbf{0}, 0)} \right] \right. \\ &\quad \left. + Q_z^2 \int_{\mathbb{R}^2} d\mathbf{r} \rho_s(\mathbf{r}, t) e^{i\mathbf{Q}_H \cdot \mathbf{r}} e^{-Q_z^2(\rho_L(\mathbf{0}, 0) - \rho_L(\mathbf{r}, t))} \right). \end{aligned} \quad (\text{V.18})$$

The first integral is the field covariance function of a smooth surface (large scale only) and thus has negligible effect in backscattering direction away from nadir. The second integral is mainly controlled by the behavior of the large-scale correlation function ρ_L at small space and time lags. Therefore, we may operate a ‘‘geometrical-optics-like’’ expansion about the origin

$$\rho_L(\mathbf{0}, 0) - \rho_L(\mathbf{r}, t) \simeq \frac{1}{2} [x, y, t] \cdot \Sigma_L \cdot [x, y, t]^T \quad (\text{V.19})$$

where the superscript T indicates the transposed vector and

$$\Sigma_L = \begin{bmatrix} \sigma_{200}^2 & \sigma_{110}^2 & \sigma_{101}^2 \\ \sigma_{110}^2 & \sigma_{020}^2 & \sigma_{011}^2 \\ \sigma_{101}^2 & \sigma_{011}^2 & \sigma_{002}^2 \end{bmatrix} \quad (\text{V.20})$$

is the spatiotemporal covariance matrix of large-scale slopes. Its elements

$$\sigma_{\alpha\beta\nu}^2 = - \left. \frac{\partial^2 \rho_L}{\partial x^\alpha \partial y^\beta \partial t^\nu} \right|_{\mathbf{r}=\mathbf{0}, t=0} \quad (\text{V.21})$$

are the cross mean square slopes with respect to the space and time variables. After Fourier transform, we obtain the Doppler spectrum

$$\begin{aligned} D(\omega) &\propto \int_{\mathbb{R}^3} dt d\mathbf{r} e^{i\mathbf{Q}_H \cdot \mathbf{r}} e^{-i\omega t} \rho_s(\mathbf{r}, t) \\ &\times \exp \left(-\frac{1}{2} Q_z^2 [\mathbf{r}, t]^T \cdot \Sigma_L \cdot [\mathbf{r}, t] \right) \end{aligned} \quad (\text{V.22})$$

which can conveniently be rewritten as a convolution integral

$$D(\omega) \propto \int_{\mathbb{R}^3} d\mathbf{k}' d\omega' \widehat{\rho}_s(\mathbf{k}', \omega') P_{Q_z^2 \Sigma_L}(\mathbf{Q}_H - \mathbf{k}', \omega - \omega'). \quad (\text{V.23})$$

Here, we have introduced $P_{Q_z^2 \Sigma_L}$ as the 3-D Gaussian centered probability density with subscripted covariance matrix

$$P_{Q_z^2 \Sigma_L}(\mathbf{u}, v) = \frac{1}{(2\pi |Q_z^2 \Sigma_L|)^{3/2}} \exp\left(-\frac{1}{2Q_z^2} [\mathbf{u}, v]^T \cdot \Sigma_L^{-1} \cdot [\mathbf{u}, v]\right) \quad (\text{V.24})$$

and $\widehat{\rho}_s$ as the 3-D Fourier transform of the surface covariance function

$$\widehat{\rho}_s(\mathbf{k}, \omega) = \frac{1}{(2\pi)^3} \int_{\mathbb{R}^3} dt d\mathbf{r} e^{-i\mathbf{k}\cdot\mathbf{r}} e^{-i\omega t} \rho_s(\mathbf{r}, t). \quad (\text{V.25})$$

This leads to a reduction of the Doppler spectrum

$$D(\omega) \propto \int_{\mathbb{R}^2} d\mathbf{k}' \Gamma_{as}(\mathbf{k}') P_{Q_z^2 \Sigma_L}(\mathbf{Q}_H - \mathbf{k}', \omega - \omega_{\mathbf{k}'}) + \int_{\mathbb{R}^2} d\mathbf{k}' \Gamma_{as}(-\mathbf{k}') P_{Q_z^2 \Sigma_L}(\mathbf{Q}_H - \mathbf{k}', \omega + \omega_{\mathbf{k}'}) \quad (\text{V.26})$$

where $\omega_{\mathbf{k}'} = \sqrt{g|\mathbf{k}'|(1 + |\mathbf{k}'|^2/k_M^2)}$. In the case of half-sided spectra, we may restrict the wavenumbers \mathbf{k} to the half-plane $\mathbf{k} \cdot \widehat{\mathbf{K}}_0 < 0$, i.e., we may assume that Γ_{as} vanishes over the half-space $\mathbf{k} \cdot \widehat{\mathbf{K}}_0 > 0$. Hence, we can rewrite the Doppler spectrum in terms of centrosymmetric spectrum $\Gamma_s(\mathbf{k}) = \Gamma_{as}(\mathbf{k}) + \Gamma_{as}(-\mathbf{k})$

$$D(\omega) \propto \int_{\mathbb{R}^2} d\mathbf{k} \Gamma_s(\mathbf{k}) P_{Q_z^2 \Sigma_L}(\mathbf{Q}_H - \mathbf{k}, \omega + \text{sgn}(\widehat{\mathbf{k}} \cdot \widehat{\mathbf{K}}_0) \omega_{\mathbf{k}}) \quad (\text{V.27})$$

and the same for the elements of the covariance matrix

$$\sigma_{\alpha\beta\nu}^2 = \int_{\mathbb{R}^2} (\text{sgn}(\widehat{\mathbf{k}} \cdot \widehat{\mathbf{K}}_0) \omega_{\mathbf{k}})^\nu k_x^\alpha k_y^\beta \Gamma_L(\mathbf{k}) dk_x dk_y. \quad (\text{V.28})$$

After some algebraic manipulations, the first two moments of the Doppler spectrum can be easily extracted. Altogether, we obtain (we have dropped the $\widehat{\mathbf{K}}_0$ variable using the replacement $\widehat{\mathbf{Q}}_H = -\widehat{\mathbf{K}}_0$)

$$\begin{aligned} \omega_c &= A^{-1} \int_{\mathbb{R}^2} d\mathbf{k} \Gamma_s(\mathbf{k}) P(\mathbf{Q}_H - \mathbf{k}) \\ &\quad \times \left(\text{sgn}(\widehat{\mathbf{k}} \cdot \widehat{\mathbf{Q}}_H) \omega_{\mathbf{k}} + (\mathbb{M}\mathbf{T}) \cdot (\mathbf{Q}_H - \mathbf{k}) \right) \quad (\text{V.29}) \\ (2\pi\gamma)^2 + \omega_c^2 &= A^{-1} \int_{\mathbb{R}^2} d\mathbf{k} \Gamma_s(\mathbf{k}) P(\mathbf{Q}_H - \mathbf{k}) \end{aligned}$$

$$\times \left(\chi Q_z^2 + \left[\text{sgn}(\widehat{\mathbf{k}} \cdot \widehat{\mathbf{Q}}_H) \omega_{\mathbf{k}} + (\mathbb{M}\mathbf{T}) \cdot (\mathbf{Q}_H - \mathbf{k}) \right]^2 \right) \quad (\text{V.30})$$

with

$$A = \int d\mathbf{k} \Gamma_s(\mathbf{k}) P(\mathbf{Q}_H - \mathbf{k}). \quad (\text{V.31})$$

Here, we have written P for the 2-D Gaussian with covariance symmetric matrix $Q_z^{-2}\mathbb{M}$, where

$$\begin{aligned} \mathbb{M} &= \begin{bmatrix} \sigma_{200}^2 & \sigma_{110}^2 \\ \sigma_{110}^2 & \sigma_{020}^2 \end{bmatrix}^{-1} & \chi &= |\Sigma_L| |\mathbb{M}| = \sigma_{002}^2 - \mathbf{T}^T \mathbb{M} \mathbf{T} \\ \mathbf{T} &= [\sigma_{101}^2 \quad \sigma_{011}^2]^T. \end{aligned} \quad (\text{V.32})$$

These expressions for the position and width of the Doppler spectrum are much simpler to evaluate numerically than (IV.12) and (IV.13) derived in the framework of KA, as they do not require the computation of the spatiotemporal covariance function. They merely involve the small-scale spectrum (Γ_s) and some moments of the large-scale spectrum (Γ_L). For 1-D surfaces, the quantities \mathbb{M} , \mathbf{T} , and χ reduce to $1/\sigma_{20}^2$, σ_{11}^2 , and $(\sigma_{20}^2 \sigma_{02}^2 - \sigma_{11}^4)/\sigma_{20}^2$, respectively, with the notation

$$\sigma_{\alpha\nu}^2 = \int_{\mathbb{R}} k^\alpha (\text{sgn}(k) \omega_k)^\nu \Gamma_L(k) dk \quad (\text{V.33})$$

for the signed moments of the spectrum. The expressions (V.29) and (V.30) can be further simplified whenever the components of \mathbb{M}^{-1} are very small compared to unity, which is usually the case since they have the order of magnitude of mean square slopes. In that case, the Gaussian term P is a sharp peak about the Bragg frequency, over which the spectrum can be supposed to be slowly varying. Mathematically, this means that the Gaussian integrand and its polynomial factor can be replaced by a combination of delta functions and their derivative about the Bragg wavenumber \mathbf{Q}_H . Tedious but straightforward calculations lead to

$$\omega_c = \omega_{\mathbf{Q}_H} - Q_z^2 \frac{[\nabla_{\mathbf{k}} \Gamma_s](\mathbf{Q}_H)}{\Gamma_s(\mathbf{Q}_H)} \cdot \mathbf{T} \quad (\text{V.34})$$

$$\begin{aligned} (2\pi\gamma)^2 &= Q_z^2 \left(\sigma_{002}^2 - \widehat{\mathbf{Q}}_H \cdot \mathbf{T} \left(\frac{g(1 + 3|\mathbf{Q}_H|^2/k_M^2)}{\omega_{\mathbf{Q}_H}} \right) \right. \\ &\quad \left. + Q_z^2 \mathbf{T}^T \cdot \nabla_{\mathbf{k}} \left[\frac{\nabla_{\mathbf{k}} \Gamma_s}{\Gamma_s} \right]_{\mathbf{k}=\mathbf{Q}_H} \cdot \mathbf{T} \right) \quad (\text{V.35}) \end{aligned}$$

where $\omega_{\mathbf{Q}_H} = \sqrt{g|\mathbf{Q}_H|(1 + |\mathbf{Q}_H|^2/k_M^2)}$ is the free Bragg wave pulsation and $\nabla_{\mathbf{k}}$ is the gradient operator relative to the wavenumber variable. These simple formulas show that, under the TSM starting from the KA, the main Doppler characteristics only depend on the level and shape of the wavenumber spectrum at the Bragg vector. To distinguish them from the previous TSM approximation (V.29) and (V.30), we will refer to this new set of equations as the Dirac function in the TSM (D-TSM) approximation, as a further Dirac approximation is employed to reduce the integral.

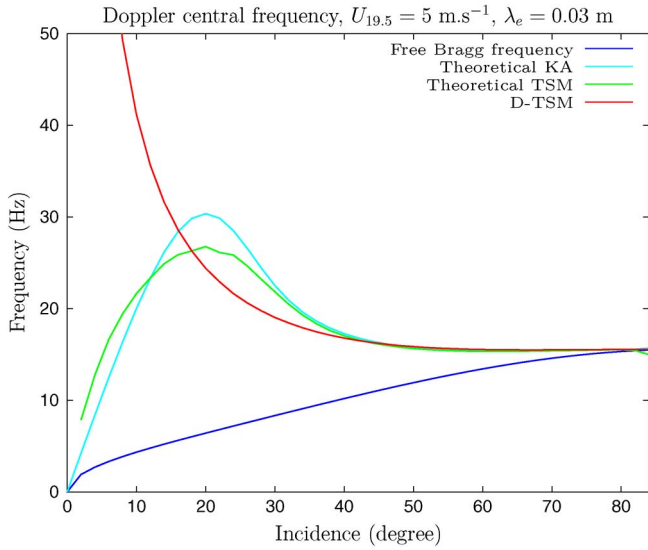


Fig. 3. Comparison of KA, TSM, and D-TSM Doppler central frequencies in X-band with $U_{19.5} = 5 \text{ m} \cdot \text{s}^{-1}$.

To ease the interpretation, let us focus again on 1-D surfaces, and suppose that the sea surface wavenumber spectrum can be locally approximated by a power law in the region of Bragg's wavenumber

$$\Gamma(k) \sim k^{-\mu}. \quad (\text{V.36})$$

Then, the approximate Doppler central frequency and width reduce to

$$f_c = \frac{1}{2\pi} \left(\omega_{Q_H} + \mu \frac{Q_z^2 \sigma_{11}^2}{Q_H} \right) \quad (\text{V.37})$$

$$\gamma = \frac{1}{2\pi} \sqrt{Q_z^2 \left(\sigma_{02}^2 - g \sigma_{11}^2 \left(\frac{1 + 3Q_H^2/k_M^2}{\omega_{Q_H}} \right) + \mu \sigma_{11}^4 \frac{Q_z^2}{Q_H^2} \right)}. \quad (\text{V.38})$$

Formula (V.37) means that the free Bragg frequency is increased by the contribution of large scales through the moment σ_{11}^2 . To understand the occurrence of the latter, it is illuminating to consider the case of a single sinusoidal large wave, for example, $\Gamma_L(k) = H^2 \delta(k - k_p)$. Then, $\sigma_{11}^2 = H^2 k_p \omega_p = H^2 k_p^2 c_p$, where c_p is the phase speed of the large wave. Thus, the Doppler shift with respect to the free Bragg frequency is proportional to the phase speed of the large wave, weighted by an angular factor $\cos^2(\theta)/\sin \theta$. Note that this factor blows up at normal incidence. This is, however, not problematic because the formula is not applicable at small incidence where the conditions of reduction of the integrals (V.29) and (V.30) are not met.

Figs. 3 and 4 show the Doppler centroid and width for the three levels of approximation: 1-D versions of (IV.12) and (IV.13) for the KA, the simplified formulas (V.29) and (V.30) arising from the TSM, and the ultimate approximations (V.37) and (V.38) obtained in assimilating the Gaussian integrand to a D-TSM with $\mu = 3$. The wavenumber cutoff between short

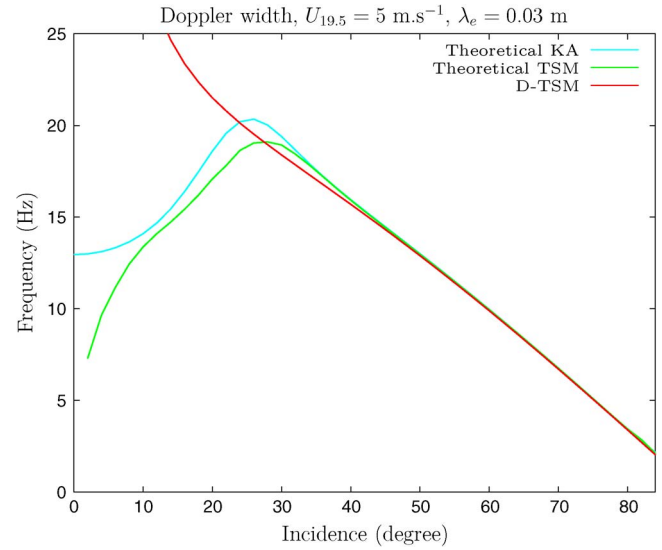


Fig. 4. Comparison of KA, TSM, and D-TSM Doppler widths in X-band with $U_{19.5} = 5 \text{ m} \cdot \text{s}^{-1}$.

and long waves is taken to be $k_c = Q_H/5$ for both TSM and D-TSM, a value which we have numerically checked to validate the TSM (V.18).

The KA and TSM approximations are in good agreement and reveal a nonmonotonic behavior for both the central frequency and width of the Doppler spectrum. At $5 \text{ m} \cdot \text{s}^{-1}$ wind speed, these quantities reach a maximum of about 25° , as already noticed in [11] and [17], and recover the free Bragg frequency position ($f_B = (2\pi)^{-1} \sqrt{g Q_H (1 + Q_H^2/k_M^2)}$) and width ($\gamma_B = 0$) at higher incidence angles. The D-TSM approximation is found to be accurate for incidence angles greater than 45° in X-band, as in L-band (not shown here). This makes the latter approximation valuable in view of its simplicity. Note that TSM shows a correct behavior even at small incidence angles. This is to be expected, as the TSM is expected to be a good approximation to the KA from which it is derived. In this respect, an angle-dependent value of the separation frequency between large and small scales is crucial (namely, $k_c = Q_H/5$), as it allows to take into account larger scales for the KA term in the nadiral region.

We note that the Kirchhoff kernel \mathbb{K} does not appear in the expressions of either f_c or γ . Consequently, any approximate scattering model with the same roughness dependence as the KA NRCS (IV.8) will yield identical expressions. This is the case, in particular, for the first-order small-slope approximation (SSA1, [20])

$$\mathbb{S}_{\text{SSA1}}(t) = \frac{\mathbb{B}}{Q_z} \int_{\mathbb{R}^2} \frac{d\mathbf{r}}{(2\pi)^2} e^{i\mathbf{Q}_H \cdot \mathbf{r}} e^{iQ_z \eta(\mathbf{r}, t)} \quad (\text{V.39})$$

which is identical to KA with the Kirchhoff kernel (\mathbb{K}) replaced by Bragg's kernel (\mathbb{B} ; see [8]). Moreover, KA and thus SSA1 are insensitive to polarization, which means that they predict the same normalized Doppler spectrum for both vertical (VV) and horizontal (HH) polarizations, an important limitation of the methods.

VI. WCA

The KA is known to be accurate at small angles and to be insensitive to polarization effects. In order to extend our methodology to larger angles and to estimate the polarization dependence of the Doppler spectrum, we use the so-called WCA. Recently revisited by Guérin *et al.* [16], this approximation introduced in [14] was shown capable to predict reasonably the NRCS from rough surfaces for both polarizations to about 80° incidence angle. The scattering amplitude in the WCA [16] writes as a correction to the tangent plane approximation in the form of a Kirchhoff integral involving second-order spatial derivatives of the surface (i.e., essentially, its curvatures)

$$\mathbb{S}_{\text{WCA}}(t) = \mathbb{S}_{\text{KA}}(t) + i \frac{\mathbb{T}}{Q_H^2} \int_{\mathbb{R}^2} \frac{d\mathbf{r}}{(2\pi)^2} \Delta\eta(\mathbf{r}, t) e^{i\mathbf{Q}_H \cdot \mathbf{r}} e^{iQ_z \eta(\mathbf{r}, t)} \quad (\text{VI.40})$$

where the kernel $\mathbb{T} = \mathbb{B} - \mathbb{K}$ is the difference between the Bragg and Kirchhoff kernels and $\Delta\eta$ is the spatial Laplacian of the surface. For 2-D surfaces, the second-order differential operator involved in the Kirchhoff integral can actually take a more general form than a mere Laplacian. However, for sea surfaces, all admissible operators have been shown in [16] to yield equivalent values for the NRCS (the so-called universal WCA), so that we will adopt the Laplacian kernel for simplicity. For 1-D surfaces, there is no such ambiguity, as all admissible second-order differential operators reduce to a second-order spatial derivative (η'') of the surface

$$\mathbb{S}_{\text{WCA}}(t) = \mathbb{S}_{\text{KA}}(t) + i \frac{\mathbb{T}}{Q_H^2} \int_{\mathbb{R}} \frac{dx}{2\pi} \eta''(x, t) e^{iQ_H x} e^{iQ_z \eta(x, t)}. \quad (\text{VI.41})$$

An alternative equivalent expression of the WCA scattering amplitude can be obtained through an integration by part, which transforms the second derivative into a square slope (η')²

$$\mathbb{S}_{\text{WCA}}(t) = \mathbb{S}_{\text{SSA}}(t) - \frac{Q_z \mathbb{T}}{Q_H^2} \int_{\mathbb{R}} \frac{dx}{2\pi} (\eta'(x, t))^2 e^{iQ_H x} e^{iQ_z \eta(x, t)}. \quad (\text{VI.42})$$

This formulation was found advantageous for the statistical calculation of NRCS and for the numerical evaluation of the scattering amplitude on deterministic surfaces (because it is difficult to compute accurately the second-order derivative, particularly in the case of sharp crests). For simplicity, we will present the statistical calculations pertaining to the WCA approximation for 1-D linear surfaces. We actually could derive a general analytical formulation for 2-D surfaces, but its technical complexity makes it too heavy to present in the context of this paper and is left for specific subsequent applications.

Starting from the alternative representation (VI.42) and using standard properties of Gaussian processes recalled in Appendix A, we obtain the following expression for the field covariance function:

$$C_{\text{WCA}}(t) = C_{\text{SSA}}(t) + \frac{2\Re e(\mathbb{T}\mathbb{T}^*)}{Q_H^2}$$

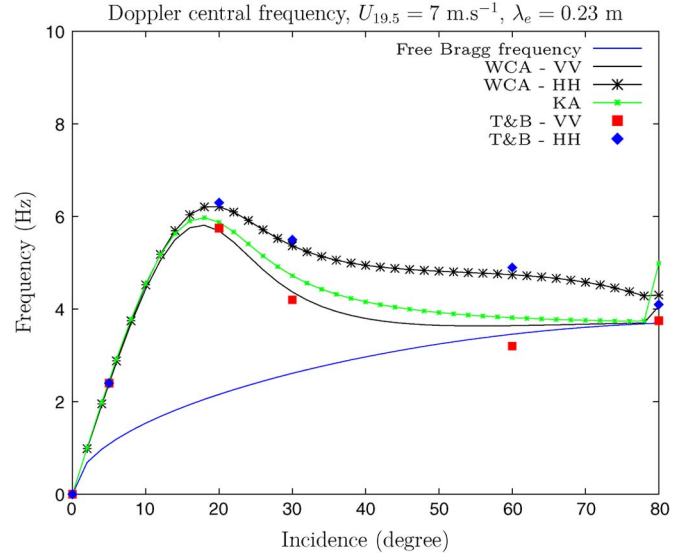


Fig. 5. Comparison of WCA vertical (VV) and horizontal (HH) polarizations and KA Doppler central frequencies in L-band with $U_{19.5} = 7 \text{ m} \cdot \text{s}^{-1}$. (T&B) Toporkov and Brown results obtained with the exact electromagnetic MOMI.

$$\begin{aligned} & \times \int_{\mathbb{R}} dx e^{iQ_H x} \left[(Q_z^2 \rho'^2 - \sigma_{20}^2) e^{-Q_z^2 S_0/2} \right. \\ & \quad \left. + \sigma_{20}^2 e^{-Q_z^2 \rho(0,0)} \right] \\ & + \frac{Q_z^2 |\mathbb{T}|^2}{Q_H^4} \int_{\mathbb{R}} dx e^{iQ_H x} \\ & \quad \times \left\{ \left[2\rho'' (\rho'' + 2Q_z^2 \rho'^2) + (Q_z^2 \rho'^2 - \sigma_{20}^2)^2 \right] \right. \\ & \quad \left. \times e^{-Q_z^2 S_0/2} - \sigma_{20}^4 e^{-Q_z^2 \rho(0,0)} \right\}. \quad (\text{VI.43}) \end{aligned}$$

The first term on the right-hand side is the field covariance function arising from SSA1 (i.e., (IV.9) with \mathbb{K} replaced by \mathbb{B}). The functions ρ' and ρ'' are the first two space derivatives of the covariance function, respectively, $\sigma_{20}^2 = -\rho''(0, 0)$ is the mean square slope, and $S_0 = 2(\rho(0, 0) - \rho(x, t))$ is the structure function of elevations. We did not derive direct analytical solutions of f_c and γ as in the KA framework [(IV.12) and (IV.13)], as this was found too complicated. Instead, we computed the time-dependent functions arising under the integral (VI.43) and evaluated the associated Doppler spectrum through a Fourier transform, as well as its first two moments (II.3). See Appendix B for numerical details. When evaluating the Doppler spectrum through a numerical time integration, it is crucial to ensure that the time interval is large enough, in order to avoid artificial broadening of the central peak. This might be an issue in working with the experimental data sets since the coherence time is limited. However, we ignore this effect in this theoretical study, which does not claim to simulate a realistic field experiment. Figs. 5 and 6 show the central frequency and width obtained with a PM sea spectrum at $U_{19.5} = 7 \text{ m} \cdot \text{s}^{-1}$ wind speed in L-band (electromagnetic wavelength $\lambda_e = 0.23 \text{ m}$). Superimposed are Toporkov and Brown [17] results obtained

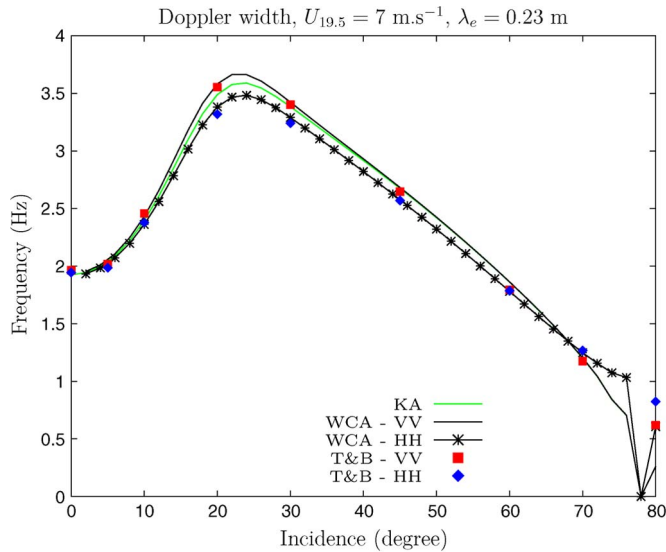


Fig. 6. Comparison of WCA vertical (VV) and horizontal (HH) polarization and KA Doppler widths in L-band with $U_{19.5} = 7 \text{ m} \cdot \text{s}^{-1}$. (T&B) Toporkov and Brown results obtained with the exact electromagnetic MOMI.

in the same conditions, with the exact electromagnetic Method of Ordered Multiple Interactions (MOMI) and Monte Carlo average on deterministic time-evolving surfaces. The data sets from [17] have been kindly provided to us by J. Toporkov, with an increased number of incidence angles and statistically more robust computations. We can observe an excellent agreement for both polarizations on the whole range of incidence. Again, the central Doppler frequency is well above the free Bragg frequency, the latter being recovered at grazing incidences. A marked polarization sensibility is apparent, with higher mean Doppler shifts in horizontal polarization, as it is classically observed. The shift in horizontal polarization can be understood by some qualitative arguments. The mean Doppler speed can be seen as an average of the phase speed of the different rough facets on the sea surface, weighted by their scattering cross section. The WCA recovers a Bragg mechanism at large incidence, where the horizontal polarization is much lower than the vertical one. The relative contribution of the ripples (small speed) is therefore weaker in horizontal polarization, so that more weight is given to larger (and faster) waves in the mean Doppler speed, thus increasing the latter.

VII. CONCLUSION

This paper has investigated the characteristics of the microwave sea Doppler spectrum in the framework of analytical electromagnetic and hydrodynamic models. Processing these models in increasing order of complexity, we have derived the first two moments of the Doppler spectrum in the framework of the KA, its TSM formulation, and, finally, the WCA for linear surfaces. The most accurate model is the WCA, which is sensitive to polarization and still enjoys a statistical numerically efficient formulation. It is robust to incidence and remains reasonably accurate until about 80° . Doppler spectra in the microwave regime are quite different from those observed with HF radio waves. Their central frequency is higher than the

free Bragg frequency, is polarization dependent, and has a non-monotonic behavior with incidence. The assumption of linear seas, however, misses an important well-known characteristic of the observed Doppler spectra, i.e., their broadening at large incidence angles. This will be corrected in a companion paper, where nonlinear hydrodynamic effects will be included.

APPENDIX A CHARACTERISTIC FUNCTIONS AND RELATED CORRELATORS

In order to calculate the statistical expressions of the WCA and its equivalent nonlinear one, we need to evaluate the complex functions of Gaussian processes. The following intermediate results are given to help the reader who would like additional calculation steps. The bracket symbols $\langle \cdot \rangle$ mean the statistical average over realizations. We suppose the surface elevation η defined by

$$\eta(x, t) = \int_{\mathbb{R}} \sqrt{\Gamma(k)} e^{i\phi_k} e^{ikx - i\text{sgn}(k)\omega_k t} dk \quad (\text{A.44})$$

where Γ is the well-known wavenumber sea spectrum and ϕ_k denotes the random phases. The prime superscript means the space derivation, and the “0” subscript means that quantities are taken at space and time origins. As an example, D'_0 means the space derivative of the displacement D taken at $t = 0$ and $x = 0$. η , η' , D , and D' are thus centered Gaussian processes and tedious, but straightforward calculations lead to

$$\langle e^{iQ_z(\eta-\eta_0)} \rangle = e^{-Q_z^2 S_0/2} \quad (\text{A.45})$$

$$\langle \eta'^2 e^{iQ_z(\eta-\eta_0)} \rangle = (Q_z^2 \rho'^2 + \sigma_2^2) e^{-Q_z^2 S_0/2} \quad (\text{A.46})$$

$$\begin{aligned} \langle \eta'^2 \eta_0'^2 e^{iQ_z(\eta-\eta_0)} \rangle &= [2\rho''(\rho'' + 2Q_z^2 \rho'^2) \\ &\quad + (Q_z^2 \rho'^2 - \sigma_2^2)^2] e^{-Q_z^2 S_0/2} \end{aligned} \quad (\text{A.47})$$

useful for WCA statistic calculations

APPENDIX B NUMERICAL RECIPES

In order to help the reader for numerical purposes, we report here some recipes that could help the calculations of the integrals in this paper. Here, we call “functions” all covariance functions that are Fourier transforms of the sea spectrum coupled with a kernel (e.g., ρ (III.6), $\partial_t \rho$ (IV.15), ρ' , ρ'' , ...).

The sea surface spectrum (in wavenumbers) used for these calculations is sampled over a logarithmic grid with 2^8 points between zero and five times the electromagnetic wavenumber. All spatiotemporal functions are evaluated over a logarithmic spatial grid depending on the electromagnetic wavelength. In most of the calculations, we used 2^{13} points between 0 and 600 times the electromagnetic wavelength (for which the integrand of the Kirchhoff integral is vanished).

The temporal sampling of the functions is linear since we then use a fast Fourier transform to evaluate the Doppler spectrum. Spatiotemporal symmetries of the functions are also used in order to minimize time calculations. The spatial integration of spatiotemporal Kirchoff integral [(IV.9), (VI.43), . . .] is done without any tricks while the time integration is realized through the fast Fourier transform. For Doppler evaluation at close nadir angles, only the functions' values at close zero lags are needed, and the processing time is very short (a time zero padding completion of $C(t)$ in (II.2) is used for numerical purposes). For higher incidence angles, larger lag values of the functions are needed for accurate calculations. All calculations done in this paper (except MOMI results which were provided by Dr. Toporkov) take less than few minutes on an ordinary laptop.

ACKNOWLEDGMENT

The authors would like to thank D. R. Thompson for the helpful discussions and J. V. Toporkov for providing the supplementary data.

REFERENCES

- [1] M. B. Kanevskii, *Radar Imaging of the Ocean Waves*. Oxford, U.K.: Elsevier, 2009.
- [2] B. L. Weber and D. E. Barrick, "On the nonlinear theory for gravity waves on the ocean's surface," *J. Phys. Oceanogr.*, vol. 7, no. 1, pp. 3–10, Jan. 1977.
- [3] D. E. Barrick and B. L. Weber, "On the nonlinear theory for gravity waves on the ocean's surface. Part II: Interpretation and applications," *J. Phys. Oceanogr.*, vol. 7, no. 1, pp. 11–21, Jan. 1977.
- [4] D. R. Thompson, B. L. Gotwols, and W. C. Keller, "A comparison of Ku-band Doppler measurements at 20 incidence with predictions from a time-dependent scattering model," *J. Geophys. Res.*, vol. 96, no. C3, pp. 4947–4955, 1991.
- [5] P. H. Y. Lee, J. D. Barter, K. L. Beach, C. L. Hindman, B. M. Lake, H. Rungaldier, J. C. Shelton, A. B. Williams, R. Yee, and H. C. Yuen, "X band microwave backscattering from ocean waves," *J. Geophys. Res.—Oceans*, vol. 100, no. C2, pp. 2591–2611, 1995.
- [6] P. H. Y. Lee, J. D. Barter, E. Caponi, M. Caponi, C. L. Hindman, B. M. Lake, and H. Rungaldier, "Wind-speed dependence of small-grazing-angle microwave backscatter from sea surfaces," *IEEE Trans. Antennas Propag.*, vol. 44, no. 3, pp. 333–340, Mar. 1996.
- [7] P. Forget, M. Saillard, and P. Broche, "Observations of the sea surface by coherent L band radar at low grazing angles in a nearshore environment," *J. Geophys. Res.*, vol. 111, no. C9, p. C09015, 2006.
- [8] T. Elfouhaily and C. A. Guérin, "A critical survey of approximate scattering wave theories from random rough surfaces," *Waves Random Complex Media*, vol. 14, no. 4, pp. 1–40, 2004.
- [9] D. R. Thompson, *Calculation of Microwave Doppler Spectra From the Ocean Surface With a Time-Dependent Composite Model*. Norwell, MA: Kluwer, 1989.
- [10] J. V. Toporkov and G. S. Brown, "Numerical study of the extended Kirchhoff approach and the lowest order small slope approximation for scattering from ocean-like surfaces: Doppler analysis," *IEEE Trans. Antennas Propag.*, vol. 50, no. 4, pp. 417–425, Apr. 2002.
- [11] A. A. Mouche, B. Chapron, N. Reul, and F. Collard, "Predicted Doppler shifts induced by ocean surface wave displacements using asymptotic electromagnetic wave scattering theories," *Waves Random Complex Media*, vol. 18, no. 1, pp. 185–196, 2008.
- [12] W. Yun-Hua, Z. Yan-Min, and G. Li-Xin, "Investigation on the Doppler shifts induced by 1-D ocean surface wave displacements by the first order small slope approximation theory: Comparison of hydrodynamic models," *Chin. Phys. B*, vol. 19, no. 7, p. 074103, Jul. 2010.
- [13] X. Li and X. Xu, "Scattering and Doppler spectral analysis for two-dimensional linear and nonlinear sea surfaces," *IEEE Trans. Geosci. Remote Sens.*, vol. 49, no. 2, pp. 603–611, Feb. 2011.
- [14] T. Elfouhaily, S. Guignard, R. Awadallah, and D. R. Thompson, "Local and non-local curvature approximation: A new asymptotic theory for wave scattering," *Waves Random Complex Media*, vol. 13, no. 4, pp. 321–337, 2003.
- [15] C. A. Guérin, G. Soriano, and T. Elfouhaily, "Weighted curvature approximation: Numerical tests for 2D dielectric surfaces," *Waves Random Complex Media*, vol. 14, no. 3, pp. 349–363, 2004.
- [16] C. A. Guérin, G. Soriano, and B. Chapron, "The weighted curvature approximation in scattering from sea surfaces," *Waves Random Complex Media*, vol. 20, no. 3, pp. 364–384, 2010.
- [17] J. V. Toporkov and G. S. Brown, "Numerical simulations of scattering from time-varying, randomly rough surfaces," *IEEE Trans. Geosci. Remote Sens.*, vol. 38, no. 4, pp. 1616–1625, Jul. 2000.
- [18] J. V. Toporkov, M. A. Sletten, and G. S. Brown, "Numerical scattering simulations from time-evolving ocean-like surfaces at L- and X-band: Doppler analysis and comparisons with a composite surface analytical model," in *Proc. Gen. Assem. Int. URSI*, Maastricht, The Netherlands, Aug. 2002.
- [19] P. Beckmann and A. Spizzichino, *The Scattering of Electromagnetic Waves From Rough Surfaces*. Norwood, MA: Artech House, 1987.
- [20] A. G. Voronovich, "Small-slope approximation for electromagnetic wave scattering at a rough interface of two dielectric half-spaces," *Waves Random Media*, vol. 4, no. 3, pp. 337–367, 1994.



Frédéric Nouguier was born in Chateaurenard, France, in 1982. He received the "Agrégation" and M.S. degrees in applied physics from the Ecole Normale Supérieure de Cachan, Cachan, France, in 2005 and 2006, respectively, the M.S. degree in physical methods for remote sensing from the University of Paris-Diderot, Paris, France, in 2006, and the Ph.D. degree in physics from the University of Marseille, Marseille, France, in 2009.

From 2009 to 2010, he was a Postdoctoral Fellow with the Laboratoire d'Océanographie Spatiale, Institut Français de Recherche pour l'Exploitation de la Mer, 29280 Plouzané, France, where he is currently working on synergical studies of optical and synthetic aperture radar sensor products in mesoscale and submesoscale ocean dynamics interpretation as a European Space Agency Postdoctoral Fellow.



Charles-Antoine Guérin received the B.Eng. degree from the Ecole Nationale Supérieure de l'Aéronautique et de l'Espace, Toulouse, France, in 1994 and the Ph.D. degree in theoretical physics from the University of Aix-Marseille I, Marseille, France, in 1998.

He is currently a Professor and a Researcher with the Laboratoire de Sondages Electromagnétiques de l'Environnement Terrestre (Unité Mixte de Recherche 6017), Geosciences and Remote Sensing Department, Centre National de la Recherche Scientifique/Université du Sud-Toulon-Var, La Garde, France. He is specializing in electromagnetic wave theory and its application to ocean remote sensing.



Gabriel Soriano was born in Paris, France, in 1972. He received the M.S. and Ph.D. degrees in physics from Paul Cézanne University Aix-Marseille III, Marseille, France, in 1996 and 2000, respectively.

He is currently an Associate Professor with Paul Cézanne University Aix-Marseille III. He is a Member of the Electromagnetic and Optical Remote Sensing (SEMO) Team, Institut Fresnel (Unité Mixte de Recherche 6133), Centre National de la Recherche Scientifique/Paul Cézanne University Aix-Marseille III. He works on surface scattering and associated

numerical methods.